Proceedings World Geothermal Congress 2005
Antalya, Turkey, 24-29 April 2005

Synthetic 3D Imaging of Geothermal System Using Well-Logging Data Set

Yun Teng[1] and Katsuaki Kioke[2]

[1]Graduate School of Science & Technology, Kumamoto Univ., Kurokami 2-39-1, Kumamoto 860-8555, Japan

040d9214@gsst.stud.kumamoto-u.ac.jp

[2]Dep. Civil & Environmental Eng., Kumamoto Univ., Kurokami 2-39-1, Kumamoto 860-8555, Japan

koike@gpo.kumamoto-u.ac.jp

Keywords: Well logging data, 3D imaging, Temperature model, Geologic model, Fluid flow, Hohi geothermal region

ABSTRACT

Accurate imaging of geothermal system around hot springs and fumarole manifestations from surface to deep zones is an interdisciplinary problem that contributes to geothermal resource exploration, volcanology, and geodynamics. The system is composed of various aspects including: temperature, lithology, and fracture distributions; hydrothermal fluid conditions on flow pattern, velocity, and pressure; rock physical properties of permeability, thermal conductivity, and porosity; and chemical properties of fluids and rocks. Most of these data are obtained by well logging and laboratory tests using borehole cores. In general, the distribution of geothermal wells is biased, and their data are limited in amount and depth ranges. Therefore, a sophisticated spatial modeling technique is indispensable to 3D imaging of geothermal system.

For this purpose, we developed a 3D modeling method by combining an interpolator analogous to minimization principle of mechanical potential energy and a stochastic simulation. The 22 km×18 km area in the Hohi geothermal region in central Kyushu, southwest Japan, was chosen as the test site. This area is well known to have two geothermal power stations, Hatchobaru and Otake. By applying the technique to the well logging dataset, the imaging down to 3000-m depth was successfully drawn based on the three modules: temperature modeling, geologic modeling, and parameter estimation.

1. INTRODUCTION

Geothermal has received substantial attention as an alternative energy source. For an assessment of geothermal resources, clarification of the characteristics of hydrothermal systems in deep parts around hot springs and fumarole manifestations is indispensable. In order to clarify the characteristics, accurate imaging of geothermal system from the surface to deep parts is necessary. The most reliable data for the imaging can be obtained by geothermal well logging. However, the distribution of geothermal wells is biased, and their data are limited in amount and depth ranges in general, which makes the imaging difficult.

To overcome this problem, we examined a 3D modeling method by combining an interpolator analogous to minimization principle of mechanical potential energy and a stochastic simulation. As a case study, the proposed method is applied to the Hohi geothermal region in southwest Japan for an actual problem of 3D imaging of geothermal system using well logging data. The imaging down to 3000-m depth consists of the three modules: temperature modeling, geologic modeling, and parameter estimation.

The subsurface temperature distribution is indispensable factor for assessing the magnitude and potential of geothermal reservoirs. Because the distribution is closely related to the hydrothermal fluid flows, a regional flow analysis around the target site is required for reservoir characterization. Thus, the proposed method was first applied to estimate the temperature distribution based on the temperature logging data from 107 well sites with 80 to 3,000-m lengths. After that, geologic modeling was produced based on the spatial distribution of eight main lithologic units such as volcanic and sedimentary rocks. Effects of unconformities and faults could be estimated from the model. It is also important to detect faults, because faults and continuous joints are believed to act as conduits for transporting the fluids and also as geothermal reservoirs. In order to detect the thermal characteristics of each lithologic unit and faults, the temperature distribution model was superimposed on the geologic distribution model. Finally, for elucidating the fluid flow pattern and localizing the recharge and discharge areas, the parameter for ascent flow velocity was estimated based on the temperature distribution model. These models and parameter obtained are combined to understand the characteristics of the Hohi geothermal system.

2. STUDY AREA

In the analysis, the Hohi geothermal region (HGR) situated in central Kyushu, southwest Japan (Fig. 1), known as one of the most active geothermal areas in Japan, was chosen as a study area. The HGR belongs to the eastern part of an extensive volcano-tectonic depression elongated along E-W, called the Beppu-Shimabara Graben, which was formed since the Neogene. Most faults in this area strike E-W, corresponding to the graben direction and the axis direction of the horizontal maximum compressive stress in the recent regional stress field (Shigeno *et al*., 1985). Although the number of faults striking NW-SE is small, several hot springs and volcanoes showing the conspicuous sign of high terrestrial heat on the ground surface such as the Takenoyu, the Hatchobaru, and Mt. Kuroiwa (Fig. 1), are considered to be connected by the faults trending in this direction. The Takenoyu fault is a well-known fracture zone (Fig. 1). White-colored alteration zones (solidified or clay zones), which appear on the surface, are widely distributed along the same direction as the elongation of the Takenoyu fault. Of special interest is the region around Waita volcano, particularly at the western foot of the volcano where the Takenoyu geothermal field is located. A number of zones of steaming ground and of hot water discharge can be identified in the field. According to the data reported by Kawamura (1985), there are more than 20 hot springs with temperatures ranging from 36.5 to 87.8 □, with total hot water and heat discharges of 524 ℓ/min and 1352 kJ/s, respectively.

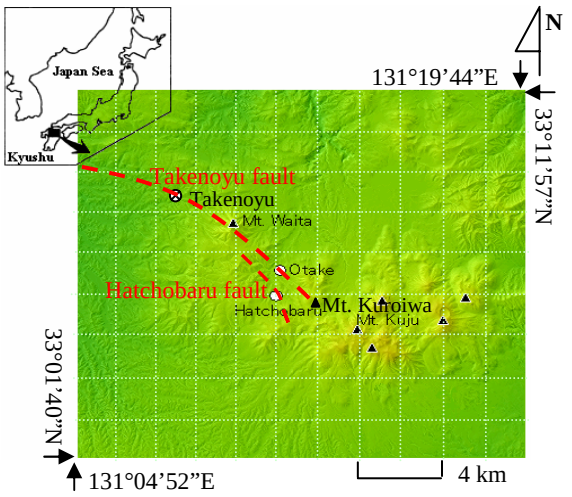

Figure 1: Location and topography of the Hohi geothermal region (HGR) in Japan. The locations of the main faults, hot springs, and volcanoes were shown. Open circles are the location of Otake and Hatchobaru geothermal power stations.

The resources in the HGR have been already utilized for power generation at two sites, Hatchobaru and Otake (Fig. 1). Furthermore, another factor making this area a favorable geothermal prospect is the presence of several zones of intense geothermal activity that have distinctive conductivity signatures at depths, due to structural or lithological factors, and especially due to the existence of remanent magma that is still undergoing a cooling process (Ehara, 1989).

3. 3D INTERPOLATION METHOD

Interpolation is used to draw contour lines automatically from sample data. Because geoscience data contain diverse spatial distribution characteristics, many interpolation methods based on different principles have been proposed (e.g., Jones *et al*., 1986). For the present analysis, a 3D optimization principle method (3DOPT) proposed by Koike *et al.* (1998) was adopted. This method is applicable for constructing directly a complicated distribution model from sample data with obscure spatial correlation and from sample data whose spatial correlation changes locally. It has been applied to various geological problems.

According to the 3DOPT, the desired 3D distribution model, f, can be obtained by minimizing the objective function Q (f; m_1, m_2, ω):

$$\begin{aligned} Q(f;m_1,m_2,\omega) = {} & m_1 \iiint \left\{ \left(\frac{\partial f}{\partial x}\right)^2 + \left(\frac{\partial f}{\partial y}\right)^2 + \left(\frac{\partial f}{\partial z}\right)^2 \right\} dxdydz \\ & + m_2 \iiint \left\{ \left(\frac{\partial^2 f}{\partial x^2}\right)^2 + \left(\frac{\partial^2 f}{\partial y^2}\right)^2 + \left(\frac{\partial^2 f}{\partial z^2}\right)^2 \right. \\ & \left. + 2\left[\left(\frac{\partial^2 f}{\partial x \partial y}\right)^2 + \left(\frac{\partial^2 f}{\partial y \partial z}\right)^2 + \left(\frac{\partial^2 f}{\partial z \partial x}\right)^2 \right] \right\} dxdydz \\ & + \omega \sum_{r=1}^{n} \{ s(x_r, y_r, z_r) - d_r \}^2 \end{aligned} \quad (1)$$

where m_1, m_2, and ω are the positive weighting coefficients, (x_r, y_r, z_r) is the coordinate of sample data (r = 1,…, n; n is the number of data), d_r represents a datum value, and s is the approximate function that is supposed to be a trilinear interpolation based on the eight grid data surrounding the sample data. The Q (f; m_1, m_2, ω) is a linear combination of the functional that evaluates the smoothness of the f and the penalty function that is the squared summation of residuals between the sample value and the estimated value. The f is dispersed by the grid data, f_{ijk} (i = 1,…, n_x; j = 1,…, n_y; k = 1,…, n_z; n_x, n_y, and n_z are grid-point numbers along the x, y, and z axes, respectively); the partial derivative terms in Eq. (1) can be replaced by difference expressions. To simplify the expression, let the dimension of mesh units be unity. In the calculation of f_{ijk}, the sample data located in the eight meshes containing the grid point ijk are used. Let the coordinate differences between the sample point (x_r, y_r, z_r) and the ijk along the x, y, and z axes be α_r, β_r, and γ_r, respectively (Fig. 2).

The f_{ijk} can be expressed in terms of the values at 25 neighboring grid point as follows:

$$\begin{aligned} f_{ijk} = {} & \frac{1}{p}[2m_2 f_{ijk-2} + 2m_2 f_{i-1jk-1} + 2m_2 f_{ij-1k-1} - (m_1 + 12m_2) f_{ijk-1} \\ & + 2m_2 f_{ij+1k-1} + 2m_2 f_{i+1jk-1} + m_2 f_{i-2jk} + 2m_2 f_{i-1j-1k} \\ & - (m_1 + 12m_2) f_{i-1jk} + 2m_2 f_{i-1j+1k} + m_2 f_{ij-2k} - (m_1 + 12m_2) f_{ij-1k} \\ & - (m_1 + 12m_2) f_{ij+1k} + m_2 f_{ij+2k} + 2m_2 f_{i+1j-1k} - (m_1 + 12m_2) f_{i+1jk} \\ & + 2m_2 f_{i+1j+1k} + m_2 f_{ijk+2} + 2m_2 f_{i-1jk+1} + 2m_2 f_{ij-1k+1} \\ & - (m_1 + 12m_2) f_{ijk+1} + 2m_2 f_{ij+1k+1} + 2m_2 f_{i+1jk+1} + m_2 f_{ijk+2} \\ & + \omega \sum_{r=1}^{n} \delta_r (1-\alpha_r^*)(1-\beta_r^*)(1-\gamma_r^*) \{ \alpha_r^* (1-\beta_r^*)(1-\gamma_r^*) f_{i+ajk} \\ & + (1-\alpha_r^*) \beta_r^* (1-\gamma_r^*) f_{ij+bk} (1-\alpha_r^*)(1-\beta_r^*) \gamma_r^* f_{ijk+c} \\ & + \alpha_r^* \beta_r^* (1-\gamma_r^*) f_{i+aj+bk} + (1-\alpha_r^*) \beta_r^* \gamma_r^* f_{ij+bk+c} + \alpha_r^* (1-\beta_r^*) \gamma_r^* f_{i+ajk+c} \\ & + \alpha_r^* \beta_r^* \gamma_r^* f_{i+aj+bk+c} - d_r \}], \end{aligned} \quad (2)$$

$$p = 6m_1 + 42m_2 + \omega \sum_{r=1}^{n} \delta_r \{(1-\alpha_r^*)(1-\beta_r^*)(1-\gamma_r^*)\}^2,$$

$$\alpha_r^* = |\alpha_r|, \quad \beta_r^* = |\beta_r|, \quad \gamma_r^* = |\gamma_r|,$$

$$a = \mathrm{sgn}(\alpha_r)1, \quad b = \mathrm{sgn}(\beta_r)1, \quad c = \mathrm{sgn}(\gamma_r)1,$$

$$\delta_r = 1 \quad \text{if} \quad 0 \le \alpha_r^*, \beta_r^* \le \gamma_r^* \le 1, \quad \text{otherwise} \quad \delta_r = 0,$$

where sgn denotes sign. The details of f_{ijk} expression that vary with grid-point location were designated by Koike *et al*. (1998). We define the values of m_1, m_2, and ωas 1, 1, and 30 in the following calculations according to the examination results by Koike *et al*. (1998).

4. APPLICATION OF 3DOPT TO TEMPERATURE DISTRIBUTION ANALYSIS

The temperature distribution is an important factor to clarify the characteristics of fluid flows and geothermal reservoirs in a geothermal area. In the HGR, many drilling investigations have been accumulated for the promotion of geothermal development since 1978. The drilling survey includes: 71 shallow drillings of 80-m and 180-m depths, 22 drillings ranging from 400 to 1000-m depth, 9 intermediate drillings ranging from 1,100 to 1,800-m depth, and 5 deep drillings ranging from 1,800 to 3,300-m depth. These are distributed irregularly in the 22 km×18 km area in the HGR (Fig. 3). The tops of logging wells in the elevations range from 400 to 1300 m.

The area was divided into an uniform grid with intervals of 250 m×250 m in the horizontal plane and 20 m in the vertical direction. A temperature distribution model was

constructed from the ground surface to the 3000-m depth. In order to represent the topography of the HGR on the model, the model was reconstructed in the form of elevation by adding the elevation value to the depth of each grid point. The results are shown by horizontal slices and vertical cross sections.

Slice maps at 100, 0, -500, and –1000-m, which are important levels to assess geothermal resources, are depicted in Figure 4. Several characteristics of temperature distribution are clarified. On the 100 and 0 m maps, two high temperature zones trending EN-WS directions are shown clearly, and the Takenoyu and Otake-Hatchobaru are found in the two zones with above 150ºC high temperature. Between the two high temperature zones, a low temperature belt trending EN-WS passes through Mt. Waita. With the increase of depth, the two high temperature zones are merging together. At the –500 and –1000 m levels, a high temperature belt trending WN-ES is formed. On the east part of Mt. Kuju, a high temperature region with above 250ºC appears.

Vertical cross sections are depicted along the N-S line passing through the Takenoyu and the E-W line passing through the Hatchobaru (Fig. 3). They provide useful information on the transfer configurations of the heat convection of the hydrothermal fluids as shown in Figure 5. Two plumes, which imply raising flows of the fluids, are seen near the Kurokawa and Takenoyu in the A-A’ section.

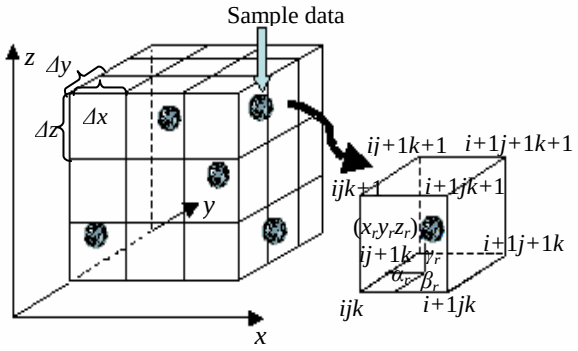

Figure 2: Setting of cubic mesh of constant spacing over the volume containing the sample data and trilinear interpolation.

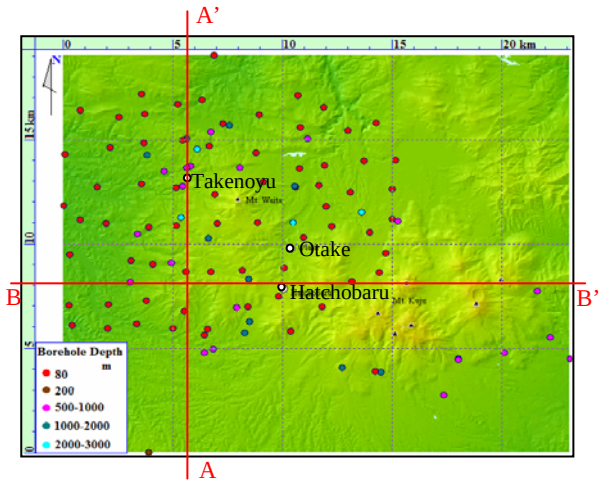

Figure 3: Distribution of borehole sites in HGR, collected for constructing temperature modeling. The dots are locations of borehole sites, and the different colors depict depth of boreholes.

The plume near the Hatcdhobaru in the B-B’ section is also seen, which may correspond to the structure of the major fracture system acting as the geothermal reservoir.

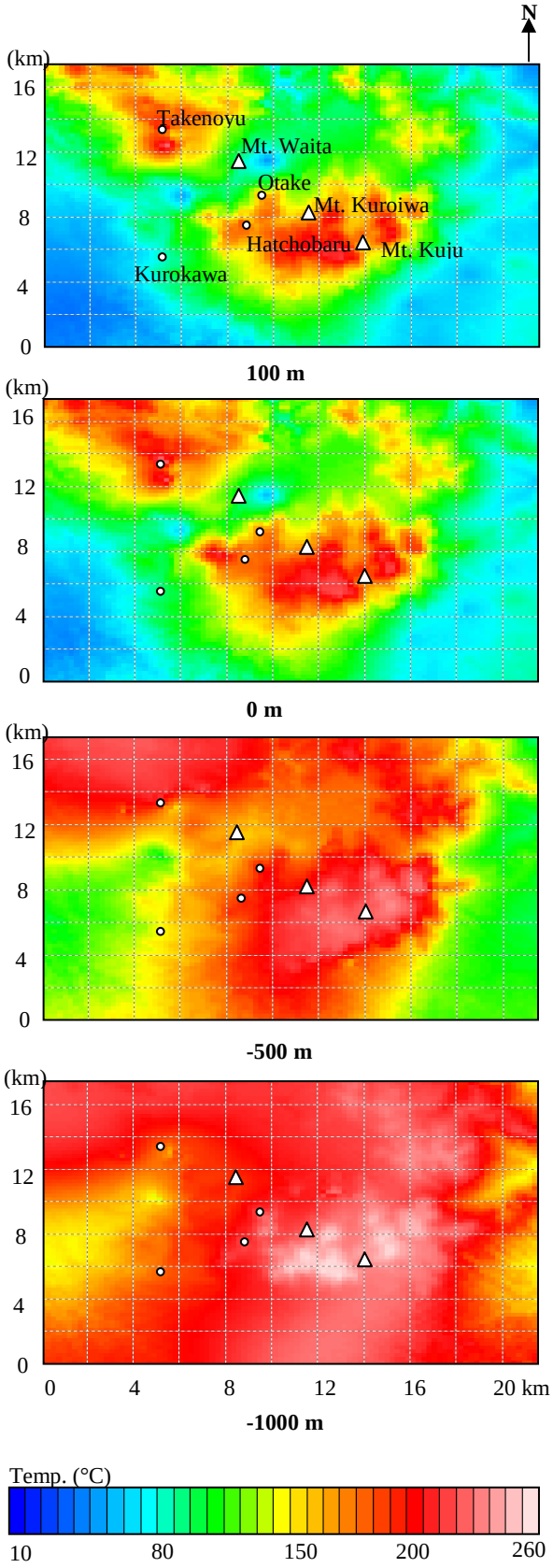

Figure 4: Horizontal temperature distributions estimated by 3DOPT at four elevations.

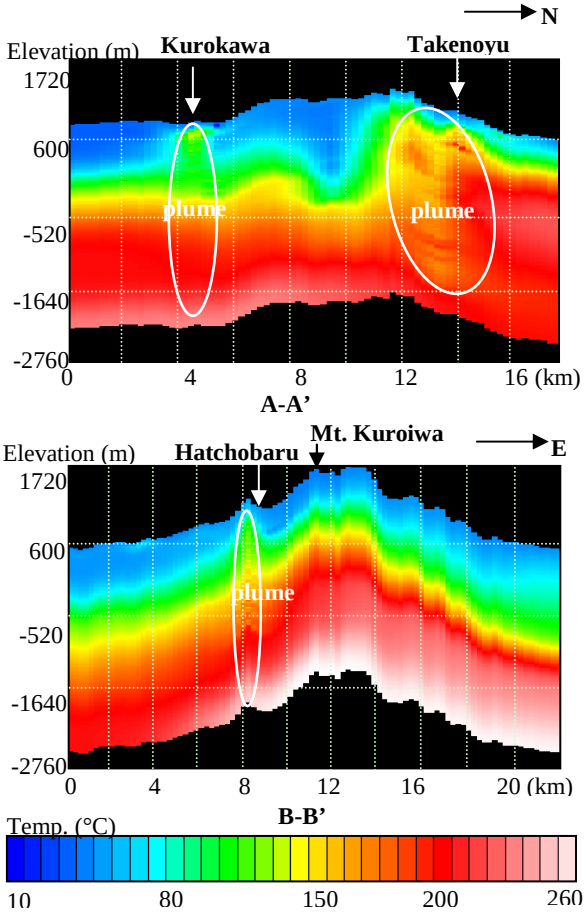

Figure 5: Vertical cross-sections showing the estimated temperature distributions along N-S (A-A') and the E-W (B-B'). These locations are depicted in Fig. 4.

In addition, for testing the effectiveness of 3DOPT, Figure 5 is compared with the temperatures (Fig. 6) estimated by a 3D finite element method based on the thermal energy balance and mass balance (Koike *et al*., 2001). These show similar trends because the plumes near the Takenoyu and Hatchobaru appear in both the figures. The numerical simulation assumes geometry, orientation, and permeability of the fracture zones. Although 3DOPT is much simpler, it can produce a plausible model.

5. GEOLOGICAL DISTRIBUTION MODEL

5.1 Modeling Method and Result

In the geological modeling, geologic logging data obtained at 21 sites in the 12 km×11 km area (Fig. 7) were used. The geology of drillhole cores was described from the viewpoint of lithofacies and geological age (Tamanyu, 1985). In the analysis, similar lithologies were combined and the time divisions were made wider to reduce the rock types. Considering the frequency of the chief lithologies in the study area, rocks are summarized into eight strata, bed rocks, Ishiba conglomerate, Taio group, Pre-Kusu altered volcanic rocks, Kusu group, Hohi volcanic rocks, young volcanic rocks, and Holocene fan and talus deposits. Geological ages are summarized into five: Paleozoic and Mesozoic, Miocene, Pliocene, Pleistocene, and Holocene. Codes are given to those strata from 1 to 8 along the geologic ages, younger to older. The resultant geologic columns of each borehole were depicted in Figure 7.

The rock code cannot be interpolated directly by 3DOPT, because the number given to each code is nominal. To overcome it, a concept of stochastic simulation using indicator was adopted (Koike *et al*., 2002). In this situation, binary transformation of each rock code into 0 or 1 is effective. The rock code 1 is first used as a criterion, and the rock data are transformed into 1 if its rock code is equal to 1 otherwise 0. 3DOPT interpolates the resultant indicators. This binary transformation and interpolation are repeated successively for the rock codes 1-8. Let the interpolated value at grid point, *ijk*, and for rock code, *l*, be $g_{ijk}^{(l)}$ ($0 \square g_{ijk}^{(l)} \square 1$; l = 1, 2, . . . , 8). The ***l**** that maximizes the $g_{ijk}^{(l)}$ is selected as the rock code at *ijk*, which is assumed to be the highest likelihood on the basis of the rock-code distribution around it.

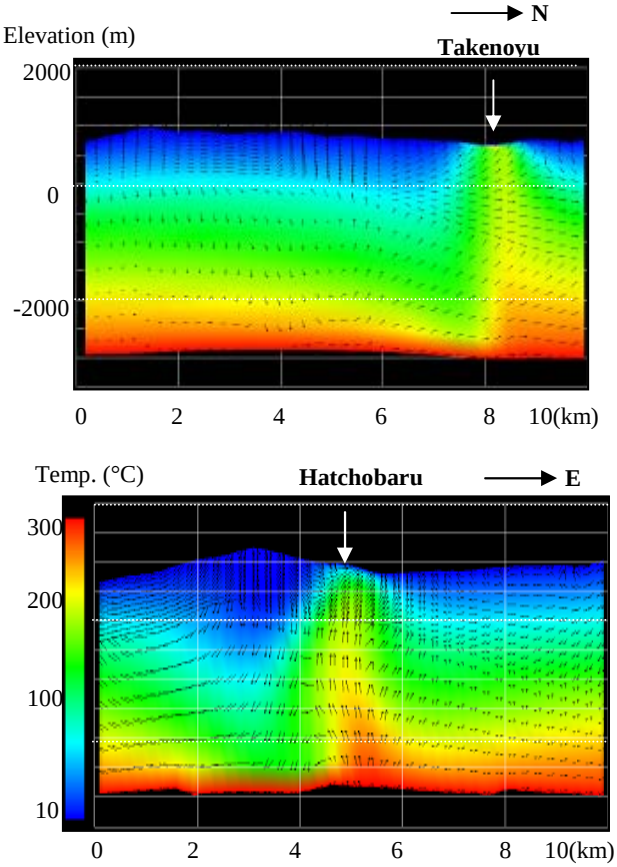

Figure 6: Vertical cross-sections showing temperature distributions and fluid flows, as estimated from a finite element method for hydrothermal fluid flow under steady state conditions.

Figure 8 depicts two E-W cross-sections for the geologic model constructed. These pass through the Takenoyu and Hatchobaru (Fig. 7). A plausible model, which shows the distribution of major lithologic units such as bedrocks, Taio group, Pre-Kusu altered vocanic rocks and Hohi volcanic rocks, was obtained in spite of the small amount and sparseness of the geologic data. It is noteworthy that the cross-sections show up the undulating folds, subsidence, upheaval, and the Takenoyu and Hatchobaru faults. It can be estimated that the Takenoyu and Hatchobaru faults were formed in late Pleistocene because the youngest stratum displaced by the faults is Hohi volcanic rocks belonging to the geologic age.

5.2 Superimposition of Geologic and Temperature Models

To detect the thermal characteristics of each lithologic unit and faults, the temperature distribution model was

superimposed on the geologic model as shown in Figure 9. The locations of vertical cross sections are the same as Figure 8. An obvious geothermal reservior is found below 700-m level in the Takenoyu fault in the A-A' cross-section and another is below 200-m level near the Hatchobaru fault in the B-B' cross-section. The temperatures of reservoirs are higher than 200□. They are mainly located in the Pliocene Pre-Kusu altered volcanic rocks and the Pleistocene Hohi volcanic rocks. The presences of the two faults act as flow channels where the hydrothermal convections occur. In the A-A' cross-section, the plume near the Takenoyu is formed because the geothermal reservoir heat the groundwater. In contrast, on the east of the Takenoyu fault, the cooler and denser groundwater is estimated. In the B-B' cross section, we can find that the groundwater on both sides of the Hachobaru fault is cooler than the groundwater along the fault. Therefore, they seem the recharge areas for the geothermal system.

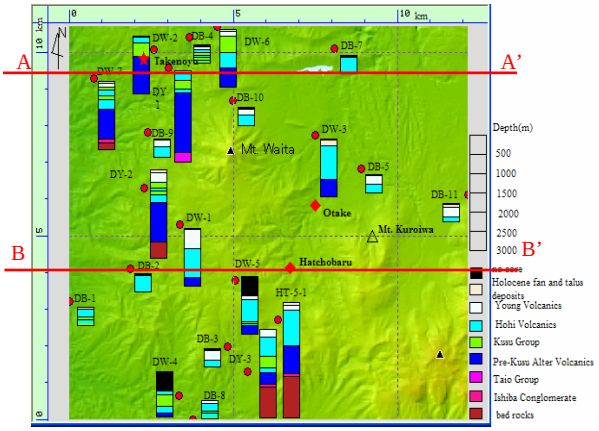

Figure 7: Simplified geologic columns with 8 lithologic units at 21 sites.

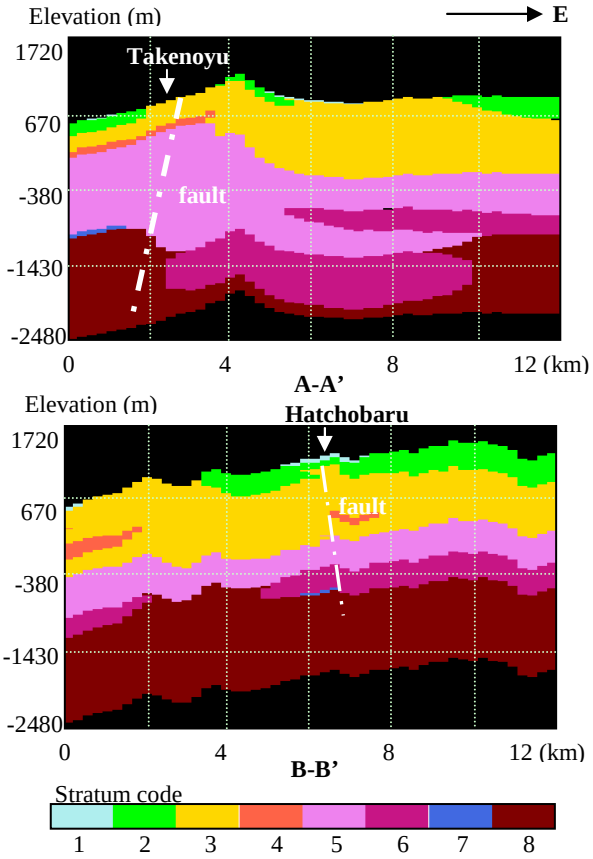

Figure 8: Vertical cross-sections of geologic distribution model along E-W lines in Fig. 7.

6. ASCENT FLOW VELOCITY MODEL

Because fluid flow velocity is another important parameter for characterizing geothermal system, the results by 3DOPT are combined with one-dimensional equation of ascending velocity. The velocity of ascending flow at the steady state in a homogeneous half-infinite porous medium can be estimated from the vertical temperature profile in the medium, under the condition that hot water ascends homogeneously and one-dimensionally from infinite depth to the ground surface. According to Turcotte and Schubert (1982, p. 401), the velocity (positive downward), v (m/s), is derived by

$$v = \frac{\lambda}{\rho c y}[\ln(T_r - T) - \ln(T_r - T_0)] \qquad (3)$$

where T_r (K) is the temperature at infinite depth, T_0 (K) is the temperature at the ground surface, ρ(kg/m^3) is the density of fluid, c (J/kg K) is the isobaric specific heat capacity of fluid, and λ (W/m K) is the thermal conductivity of the medium. We assigned the values as T_0 = 10□, T_r = 230□, λ = 4.0 W/m K, ρ= 1000 kg/m, and c = 4.185×10^3 J/kg K, respectively. T_0 and T_r were defined by the minimum and maximum temperatures by 3DOPT.

The calculation range is 20-m to 3,000-m below the surface and the temperatures in this range are substituted into Equation (3). Figure 10 shows the resultant 3D ascent flow velocity model by selecting the same location as Figures 8 and 9. We focus on the flow patterns near the Takenoyu and Hatchobaru, because these are clarified to be located in the two high temperature zones and the faults pass through the two areas from the temperature and geological distribution models. In the A-A' cross-section, the ascending flows are dominant near Takenoyu; opposite to it, much slower flows are conspicuous in the eastern part of the Takenoyu fault zone. The latter feature signifies that the flows tend to descend. Therefore, an obvious hydrothermal convection can be estimated near the Takenoyu fault. In the B-B' cross-section, a similar convection is seen between the Hatchobaru fault and the western part of the fault, although the feature is weak as compared to the Takenoyu area.

7. CONCLUSION

In order to characterize the geothermal system in the Hohi geothermal region located in the southwest Japan in detail, a spatial modeling technique, 3DOPT, was applied to the well logging dataset which consist of the temperature logging data from 107 wells and geological logging data from 21 wells. The main results are summarized as follows.

(1) The temperature distribution model successfully clarified the two high temperature zones near the Takenoyu and Otake-Hatchobaru, which are the main geothermal systems in the HGR. Geologic modeling was based on the spatial distribution of eight main lithologic units such as volcanic and sedimentary rocks. Effects of unconformities and the Takenoyu and Hatchobaru faults could be estimated from the model.

(2) By superimposition of the temperature and geologic models, thermal characteristics of each lithologic unit, faults, and geothermal reservoir were detected. The reservoirs near the Takenoyu and Otake-Hatchobaru were estimated below 700-m level and below 200-m level, respectively, which were located in the Pliocene Pre-Kusu altered volcanic rocks and the Pleistocene Hohi volcanic rocks. The temperatures in both reservoirs exceed 200□.

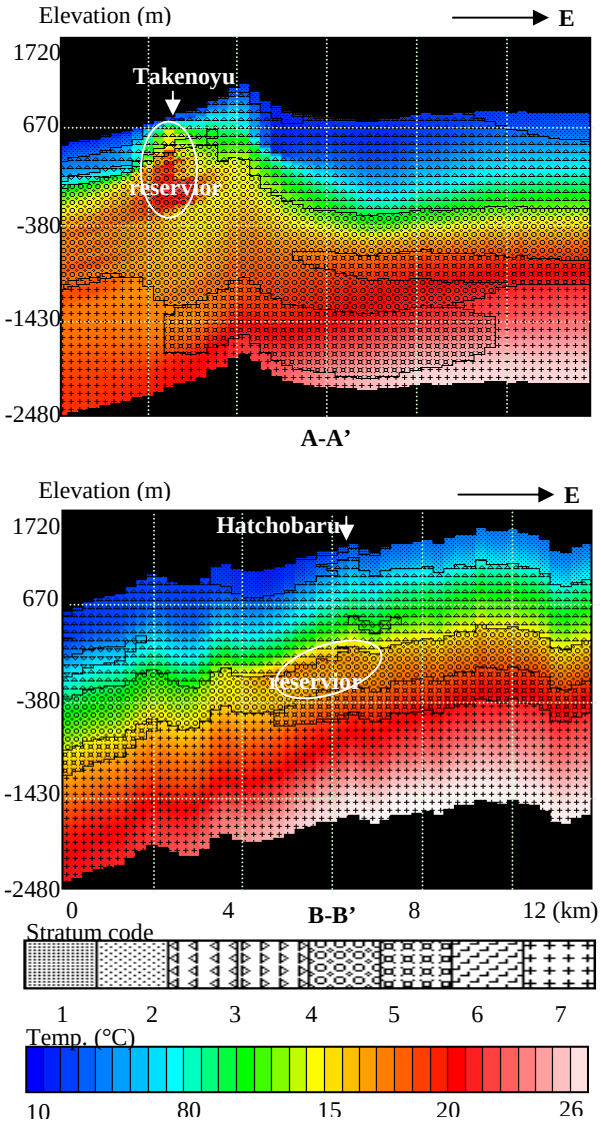

Figure 9: Vertical cross-sections by superimposing the temperature distribution model on the geologic model. The locations are shown in Fig. 7.

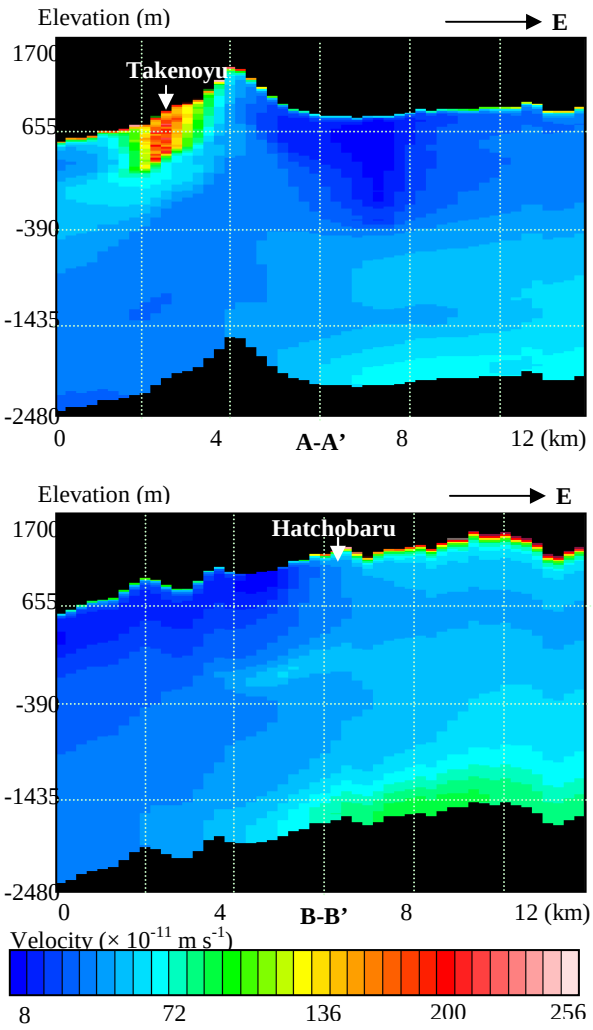

Figure 10: Vertical cross-sections showing the estimated ascent flow velocity distributions. The locations are shown in Fig. 7.

(3) The temperature distribution model could be link to estimation of the ascent flow velocity of hydrothermal fluids. The hydrothermal convection near the Takenoyu and Hatchobaru were detected. Consequently, the combination of these models and the parameter obtained are useful to understand the Hohi geothermal system.

REFERENCES

Ehara, S.: Thermal structure and seismic activity in central Kyushu, Japan, *Tectonophysics*, **159**, (1989), 269-278.

Jones, T. A., Hamilton, D. E., and Johnson, C. R.: Contouring geologic surfaces with the computer, *Van Nostrand Reinhold*, New York, (1994).

Kawamura, M.: On thermal structure of the geothermal field in Mt. Waita area, central Kyushu, Japan, *Report of the Geological Survey of Japan*, **264**, (1985), 353-382 (in Japanese with English abs.).

Koike, K., Shiraishi, Y., Verdeja, E., and Fujimura, K.: Three-dimensional interpolation and lithofacies analysis of granular composition data for earthquake-engineering characterization of shallow soil, *Mathematical Geology*, **30**, (1998), 733-759.

Koike, K., Kouda, R., and Ueki, T.: Characterizing fracture systems of Kyushu, southwest Japan, through satellite image derived lineaments superimposed on topographic and lithologic data, *Bulletin of the Geological Survey of Japan*, **52**, (2001), 405-423.

Koike, K., Matsuda, S., Suzuki, T., and Ohmi, M.: Neural network-based estimation of principal metal contents in the Hokuroku district, northern Japan, for exploring Kuroko-type deposits, *Natural Resources Research*, **11**, (2002), 135-156.

Sigeno, H., Abe, K., and Noda, T.: Conceptual hydrothermal system model for the Hohi area based on geochemistry of geothermal fluids, *Report of the Geological Survey of Japan*, **264**, (1985), 285-302 (in Japanese with English abs.).

Tamanyu, S.: Stratigraphy and geologic structures of the Hohi geothermal area, based mainly on the bore hole data: *Report of the Geological Survey of Japan*, **264,** (1985), 115-142 (in Japanese with English abs.).

Turcotte, D. L. and Schubert, G.: *Geodynamics*, Wiley, New York, (1982).